Microelectronic Engineering 98 (2012) 626–629

Contents lists available at SciVerse ScienceDirect

Microelectronic Engineering

journal homepage: www.elsevier.com/locate/mee

Nanoporous silicon nanoparticles for drug delivery applications

M. Perrone Donnorso [a,*], E. Miele [a], F. De Angelis [a,b], R. La Rocca [a], T. Limongi [a], F. Cella Zanacchi [a], S. Marras [a], R. Brescia [a], E. Di Fabrizio [a,b]

[a] Istituto Italiano di Tecnologia, Via Morego 30, 16163 Genova, Italy
[b] BIONEM lab, University of Magna Graecia, viale Europa, 88100 Germaneto, Catanzaro, Italy

ARTICLE INFO

Article history:
Available online 25 July 2012

Keywords:
Drug delivery
Nanoparticles
Nanoporous silicon
Electrochemical etching

ABSTRACT

Nanoparticles can be composed of many different types of material, however in order to be considered as suitable candidates for drug delivery purpose, they need to follow a precise tailored biological behavior. Here we propose nanoporous silicon nanoparticles as optimal nanocarriers with tunable physicochemical properties, and we present a simple few-step fabrication process and an accurate description of nanoparticles considerable features. The performed measurements show that proposed water soluble nanoparticles have excellent loading capacity with no chemical modification on the adsorbed drug. Furthermore, they can degrade releasing the carried drug in a reasonable period of time producing non toxic substances, and show photoluminescent and Raman scattering properties that are useful tools for monitoring them. Raman analyses indicate that nanoporous silicon nanoparticles are distinguished from bulk silicon by a Raman shift to low frequencies and that annealing processes at 260 °C allows to maintain intact the crystalline structure, while complete disappearance appears for annealing at 700 °C. In this way Raman spectroscopy is a useful technique to follow the changes in composition of the nanoparticles after treatments.

1. Introduction

Nanoparticles are defined as structures with diameters of few nanometers and great surface to volume ratio, that is, the ability to load, carry and release other substances. Due to these particular and important features, NPs have attracted great attention for their potential application in biomedical field [1,2], and particularly for their use in cancer treatment. Drug can be loaded into the nanoparticle's matrix by chemical and/or physical process, and once in the body, released closer to the site of action by diffusion or by degradation of the matrix. Nanoparticles can accumulate in cancer site by a passive targeting mechanism due to the enhanced permeability and retention effect (EPR) of solid tumor, or by an active targeting mechanism achieved by nanoparticles surface functionalization with tumor-specific recognition molecules. Furthermore, once on the tumor site, nanoparticles can be internalized by the cell through endocytosis process, delivering drugs in the intracellular compartments [3]. Nanoparticles can improve drug stability protecting it from rapidly clearance and can help it to cross endothelial barrier. In addition they can incorporate both hydrophilic and hydrophobic substances, improving the delivery of many poorly water-soluble anticancer drugs and allowing co-delivery of more drugs for combined therapy [4–8]. In this way nanoparticles (NPs) can enhance drug bioavailability on the cancer site improving therapeutic effect of traditional free administrated drugs, as well as reducing their toxic side effect thanks to a decrease of frequency and amount of drugs dosage.

NPs morphology (size, shape, surface) strongly affects biological behavior and must be considered in designing nanocarriers for drug delivery purpose. Non toxic, harmlessly biodegradable NPs, with size of 30–100 nm, great surface to volume ratio and high loading capacity, are optimal nanocarrier candidates in new approaches to cancer therapy [9,10]. Porous silicon (PSi) nanoparticles, considered as silicon nanoparticles having a series of voids, fulfill well these requirements [11–13] and they are promising nanocarriers in this sense.

In body fluids PSi is metabolized into non toxic silicic acid and rapidly excreted trough the urine [14]. Furthermore, the porous structure can give a great surface/volume ratio (200–800 m^2/cm^3) [15] available for drug loading and active targeting mechanism. Porosity (considered as fraction of voids in the porous structure), pore size, and morphology are related to the particles loading ability and can be tuned during the fabrication process. Porous silicon particles with high porosity formed by nanometer size interconnected open pores, have greater loading capacity efficiency and are preferable for drug delivery device.

In this paper we present the fabrication and characterization of water soluble nanoporous silicon nanoparticles (NPNPs) with size

* Corresponding author. Tel.: +39 01071781249.
E-mail addresses: michela.perrone@iit.it (M. Perrone Donnorso), francesco.deangelis@iit.it (F. De Angelis).

0167-9317/$ - see front matter © 2012 Elsevier B.V. All rights reserved.
http://dx.doi.org/10.1016/j.mee.2012.07.095

of 30–100 nm and we show preliminary investigations to test their potential application in drug delivery systems.

2. Fabrication and characterization

Nanoporous silicon nanoparticles (NPNPs) were fabricated following a top–down process consisting of few steps. In order to obtain a silicon nanoporous film, silicon wafer (resistivity 1–10 Ω cm) was anodized using an electrochemical Teflon cell in which silicon wafer (with Al contact at the bottom) acts as the anode and a platinum electrode acts as the cathode. Anodization process was performed in ethanol/HF (25%) solution (2:1 v/v), and a constant current density of 10–40 mA/cm^2 was applied for 5–10 min at 25 °C. The resulting porous films were washed in deionized water, then in ethanol and pentane, and after drying were annealed at 260 °C for 4 h to stabilize the surface. Samples were then sonicated in water for 30 min, in order to remove all the nanoporous silicon film from the bulk silicon substrate. Nanoparticles were finally obtained by ultrasonication of the nanoporous silicon film in water at 4 °C applying a power of 15 W for 5–15 min, and the resulting solution filtered through a 0.22 μm filtration membrane to eliminate larger aggregates. The desired particle size was then selected by centrifugation. NPNPs morphology, in terms of pore size and interconnectivity, porosity and particles diameter, is linked to the fabrication parameters (etching time, anodization current density, HF concentration, Si doping and ultrasonication time) and can be tuned in order to obtain the desired morphological features. In Fig. 1, we present NPNPs of 65 ± 20 nm fabricated by anodization of boron-doped silicon wafer applying a current density of 10 mA/cm^2 for 10 min in ethanol/HF (25%) solution (2:1 v/v). Ultrasonication at 15 W for 15 min and centrifugation at 12,000 rpm (11,450×g) for 40 min were performed. Recovered NPNPs were stored at 4 °C until use in order to prevent particles aggregation, since they have a great surface hydrophobicity [16] and were characterized using various complementary techniques (Fig. 1).

Porosity of 87% (rough estimation) was determined by gravimetric measurements of the silicon layer [10]. Scanning electron microscopy (SEM), Transmission electron microscopy (TEM) and Dynamic light scattering (DLS) analysis were used to determine NPNPs hydrodynamic size, while Scanning transmission electron microscopy (STEM) analysis was carried out to study the pore width (2–10 nm). SEM analysis was performed using a JEOL-JSM-7500FA high resolution microscope, equipped with a cold cathode field emission gun, operating at a voltage of 5 kV. Images were collected using an in-lens Everhard–Thornley detector with Energy Filter (R-Filter) design, which allows variable energy filtering from secondary (SE) to backscattered (BSE) electrons. Samples were prepared by depositing 100 μl of NPNPs solution onto a silicon wafer, letting the solvent evaporate in dry box overnight. For TEM analysis a JEOL-JEM1011 microscope, equipped with a thermionic source and operating at 100 kV, was used and sample were prepared by depositing 100 μl of NPNPs solution onto a copper grid covered with a thin carbon layer. STEM analyses were carried out with a JEOL-JEM2200FS microscope operating at 200 kV, equipped with CEOS image aberration corrector and high angle annular dark field (HAADF) detector.

In order to perform accurate and complete characterization of fabricated NPNPs, confocal microscopy and Raman spectroscopy were also used. Previous studies reported that these two analytical techniques are sensitive to changes in NPNPs porous structure [17–19].

Emission spectrum of porous silicon NPNPs solution, measured using confocal microscopy (A1 Confocal laser microscope, Nikon Instr) and obtained exciting NPs with near-UV radiation (405 nm), exhibits a broad emission band in the visible range centered at 565 nm (red-orange). The observed intrinsic NPNPs photoluminescent property is an interesting feature for biological application [17] and several models have been proposed to explain photoluminescent trend in NPNPs [18,19].

To further study NPNPs at nanoscale level, Raman spectroscopy analyses were performed. Raman spectroscopy measures the

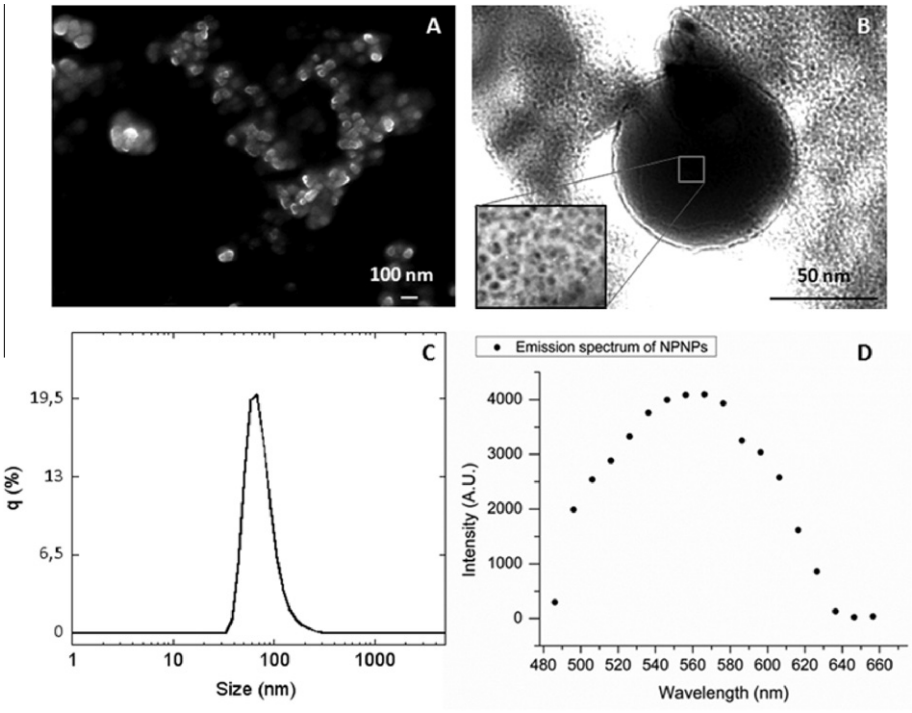

Fig. 1. SEM (A) (mag 50,000×, scale bar 100 nm) and TEM (B) (scale bar 50 nm) images, STEM–HAADF (inset) image (scale bar 50 nm), DLS size distribution (C) (Zetasizer Malvern) and emission spectrum by Confocal Microscopy (D) (objective Nikon PlanApo 60×) of 65 ± 20 nm porous silicon nanoparticles.

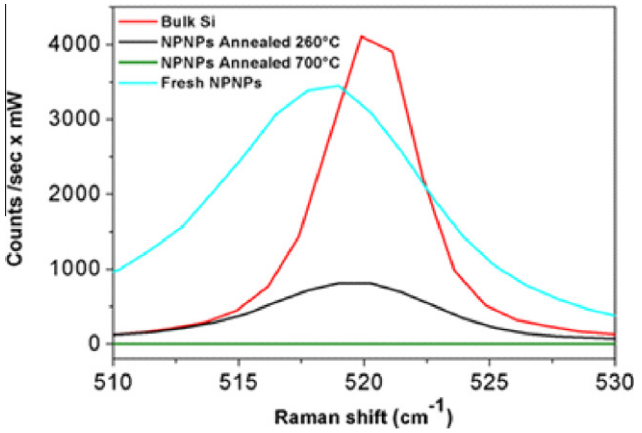

Fig. 2. Raman spectra of bulk silicon wafer, fresh NPNPs, annealed NPNPs for 4 h at 260 °C and for 1 h at 700 °C. Anodization parameters: J = 10 mA/cm^2, t_a = 10 min, HF (25%)/EtOH = 1:1:2.

vibrational frequencies of various parts of a molecule by illuminating a sample with a single wavelength of laser light and the resulting scattered light is collected and analyzed. Vibrational frequencies depend on bond strength, atomic mass of bonded atoms and other factors, including intermolecular interactions and crystalline arrangement of solids [20]. Then Raman technique can be used to quantify the relative amounts of amorphous and crystalline silicon in NPNPs. Micro-Raman analysis was performed to characterized fresh and annealed (4 h at 260 °C and 1 h at 700 °C) NPNPs (Fig. 2), depositing 2 μl of each water NPNPs suspension (100 μg/ml) on gold-sputtered based substrate [21,22] and leaving sample at room temperature for 1 h to eliminate the excess of water. Raman spectra were collected on InVia Raman microscope from Renishaw equipped with laser source at 633 nm (13-mW power) through a 50× objective (LEICA N PLAN EPI 50×/0.75). The micro-Raman spectrometer was calibrated before the measurements by using a Si wafer as a reference. Laser source at 633 nm was used since in most biomedical applications excitation in the UV region results in high-fluorescence background and can photodamage biological samples. All the Raman spectra were baseline corrected using 2-order polynomials to eliminate the autofluorescence background. Silicon–silicon bonds are symmetrical and result in strong Raman scattering. Crystalline silicon has highly uniform bond angles and bond lengths, and exists in a limited number of states. This results in sharp Raman peaks with a charac-

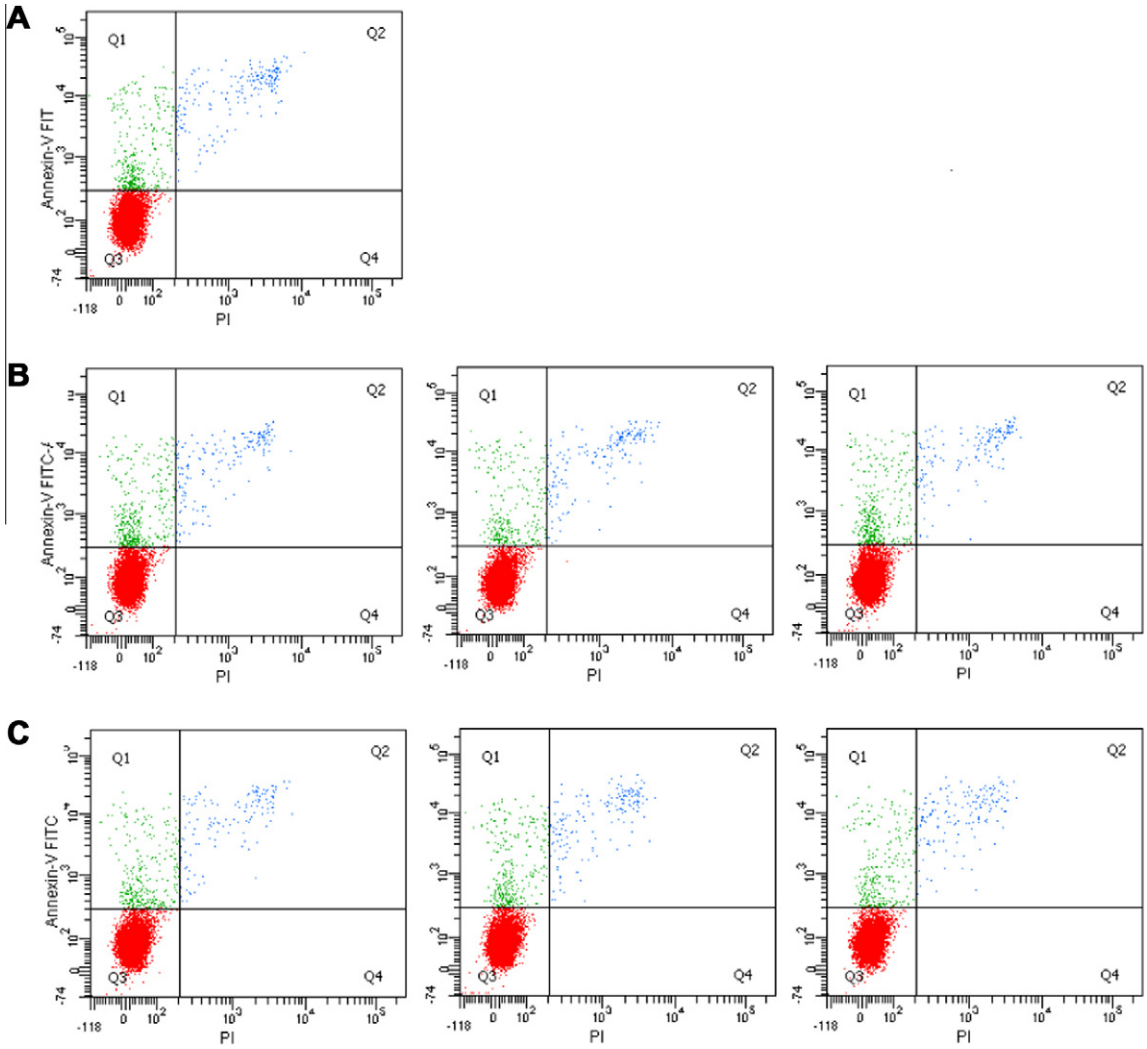

Fig. 3. Apoptosis test of THP1 cell line incubated with 100 μg (panel B) and 200 μg (panel C) of fresh NPNPs, annealed at 260 °C and annealed at 700 °C (from left to right) for 48 h at 37 °C. In panel A control sample is shown. Cells were stained with Annexin V that colors the cells in early stages of apoptosis (Q1) and Propidium Iodide (PI) that colors cells in late stages of apoptosis (Q2).

teristic strong band at 520 cm^{-1} [1](red curve in Fig. 2). Amorphous silicon in NPNPs is less ordered in its arrangement than crystalline form, since it has a wider array of bond angles, bond energies and bond lengths in addition to dangling bonds. The distribution of possible states leads to a broad Raman bands shift to low frequency side distinguishable from that of crystalline silicon (blue curve in Fig. 2).

It is known that the Si dangling bonds on the surface of fresh NPNPs consist of large amount of H atoms to form weak Si–H bonds, which are easy to be oxidized. Despite a low broad band with maximum at 480 cm^{-1} is expected as of amorphous silica (SiO_x), we were not able to observe it in our spectra probably because of not enough sensibility [23]. During thermal annealing process, the surface would immediately cover with oxygen atoms instead of H atoms, and the oxygen extent of NPNPs would increase with the prolonged time of oxidation. For annealed NPNPs at 260 °C, Raman peak at 520 cm^{-1} is almost unshifted (black curve in Fig. 2) with respect to its bulk value thanks to a bonding rearrangement that gives a structure similar to the silicon bulk. Fig. 2 shows that NPNPs annealed at 700 °C (1 h) do not exhibit at all the silicon crystalline band at 520 cm^{-1} (green curve). Since the intensity of the band centered at 520 cm^{-1} is proportional to the fraction of the crystalline phase, the observed decrease of that band intensity for annealed samples suggests that after the annealing process crystalline structure of NPNPs is not the same as before.

In order to evaluate NPNPs *in vitro* toxicity, apoptosis test (Annexin V-FITC Apoptosis Detection Kit, Abcam) on healthy monocites (THP1) and on colorectal carcinoma cell line (HCT-116) was performed. Fig. 3 shows data obtained by flow cytometry (BD FACSAria II Flow Cytometer) on THP1 cells incubated with 100 μg (panel B) and 200 μg (panel C) of three different types of NPNPs (fresh, annealed at 260 °C and annealed at 700 °C) for 48 h in RPMI 1640 medium at 37 °C at 5% CO_2. For each experiment 2×10^5 cells were used. Annexin V and iodure propidium (PI) staining was used to identify apoptotic stages by flow cytometry. Each sample was incubated with Annexin V and PI at room temperature for 10 min. Cells reacting with NPNPs were then compared with control cells treated with medium only (panel A). Percentage of apoptotic cells (panels B and C) in each sample is not statistically significant (about 4–5%) compared to the control cells (panel A), indicating no toxic effects on the cells. Similar results were obtained on colorectal carcinoma HCT-116 cells (data not shown).

To evaluate NPNPs potential in drug delivery application, drug loading test was performed incubating 100 μg of NPNPs (100 μg/ml) with 100 and 200 μg of Doxorubicin (Sigma), a widely used anticancer drug, in water at room temperature overnight. Loaded nanoparticles were centrifugated at 12,000 rpm (11,450×*g*) for 30 min and the supernatant collected and analyzed by UV–visible spectroscopy analysis to quantify the amount of incorporated drug (comparing with drug standard curve). For fabricated NPNPs of 65 nm an optimal payload was found (5% weight) and dissolution investigation showed that under physiological conditions drug embedded NPNPs dissolve in 120 h releasing the loaded drug [8].

3. Conclusion

In conclusion here we present a process for the fabrication of biocompatible, luminescent and water soluble NPNPs. Size, shape and surface chemistry of proposed NPNPs can be easily tuned operating on the fabrication parameters to achieve a desired tailored biological behavior. Furthermore, our experiments indicate that this type of nanoparticles can show efficient drug payload capacity only incubating NPNPs with desired drugs in water solution at room temperature. This suggests that drugs can be entrapped into the nanoparticles pores by a direct physical adsorption process.

Obtained confocal and Raman spectra represent the reference fingerprint of our NPNPs, and are useful tools to check NPNPs fabrication performance and their localization during cell uptake [24]. Raman spectroscopy demonstrate that annealed samples at 260 °C (4 h) still contain a relevant fraction of crystalline silicon as well as a fraction of SiO_x component, STEM analysis suggests that porous structure exists even after annealing process. Annealed NPNPs seem to have more advantages for drug delivery purpose since they can be used to load both hydrophilic and hydrophobic drugs. In addition they show higher luminescent properties, can prevent aggregation in water solution and degrade faster in physiological solution.

Finally, in this paper we showed detailed characterization of NPNPs that is crucial to assess their safety and efficacy in biomedical application. Results obtained suggest that the proposed NPNPs are suitable candidates for nanoparticles-based drug delivery systems with the aim of improving bioavailability of transported drugs. This allows to achieve an higher therapeutic index (defined as the ratio between the drug dose that produces the desired therapeutic effect and the dose that causes unwanted and possibly toxic side effects) compared to free administration of traditional drugs.

[1] For interpretation of color in Fig. 2, the reader is referred to the web version of this article.

References

[1] L. Vaccari, D. Canton, N. Zaffaroni, R. Villa, M. Tormen, E. Di Fabrizio, Microelectronic Engineering 83 (2005) 1598–1601.
[2] M. Gaspari, M.M. Cheng, R. Terracciano, X. Liu, A.J. Nijdam, L. Vaccari, E. Di Fabrizio, E.F. Petricoin, L.A. Liotta, G. Cuda, S. Venuta, M. Ferrari, Journal of Proteome Research 5 (2006) 1261–1266.
[3] L.E. van Vlerken, M.M. Amiji, Expert Opinion Drug Delivery 3 (2) (2006) 205–216.
[4] O.C. Farokhzad, R. Langer, ACS Nano 3 (1) (2009) 16–20.
[5] D. Peer, J.M. Karp, S. Hong, O.C. Farokhzad, R. Margalit, R. Langer, Nature Nanotechnology 2 (2007) 751–760.
[6] R. Pandey, G.K. Khuller, Journal of Antimicrobial Chemotherapy 54 (2004) 266–268.
[7] A. Singh, F. Dilnawaz, S. Mewar, U. Sharma, N.R. Jagannathan, S.K. Sahoo, ACS Applied Materials & Interfaces 3 (3) (2011) 842–856.
[8] F. De Angelis, A. Pujia, C. Falcone, E. Iaccino, C. Palmieri, C. Liberale, F. Mecarini, P. Candeloro, L. Luberto, A. de Laurentiis, G. Das, G. Scala, E. Di Fabrizio, Nanoscale 2 (2010) 2230–2236.
[9] R.A. Petros, J.M. DeSimone, Nature Reviews Drug Discovery 9 (2010) 615–627.
[10] S. Mitragotri, J. Lahan, Nature Materials 8 (2009) 15–23.
[11] P. Granitzer, K. Rumpf, Materials 3 (2010) 943–998.
[12] L. Canham, Properties of Porous Silicon, INSPEC – The Institution of Electrical Engineers London, United Kingdom, 1997.
[13] N. O'Farrell, A. Houlton, B.R. Horrocks, International Journal of Nanomedicine 1 (4) (2006) 451–472.
[14] J.H. Park, L. Gu, G. von Maltzahn, E. Ruoslahti, S.N. Bhatia, M.J. Sailor, Nature Materials 8 (2009) 331–336.
[15] A. Halimaoui, Porous silicon: material processing, properties and applications, in: J.C. Vial, J. Derrien (Eds.), Porous Silicon Science and Technology, Springer-Verlag, 1995.
[16] A. Pujia, F. De Angelis, D. Scumaci, M. Gaspari, C. Liberale, P. Candeloro, G. Cuda, E. Di Fabrizio, International Journal of Nanomedicine 5 (2010) 1005–1015.
[17] S.M. Janib, A.S. Moses, J.A. MacKay, Advanced Drug Delivery Reviews 62 (2010) 1052–1063.
[18] P. Kumar, ISRN, Nanotechnology 2011 (2011) http://dx.doi.org/10.5402/2011/163168.
[19] S. Godefroo, M. Hayne, M. Jivanescu, A. Stesmans, M. Zacharias, O.I. Lebedev, G. van Tendeloo, V.V. Moschchalkov, Nature Nanotechnology 3 (2008) 174–178.
[20] G. Das, F. Mecarini, F. Gentile, F. De Angelis, H.G.M. Kumar, P. Candeloro, C. Liberale, G. Cuda, E. Di Fabrizio, Biosensors and Bioelectronics 24 (2009) 1693–1699.
[21] F. De Angelis, F. Gentile, F. Mecarini, G. Das, M. Moretti, P. Candeloro, M.L. Coluccio, G. Cojoc, A. Accardo, C. Liberale, R.P. Zaccaria, G. Perozziello, L. Tirinato, A. Toma, G. Cuda, R. Cingolani, E. Di Fabrizio, Nature Photonics (in press), http://dx.doi.org/10.1038/nphoton.2011.222.
[22] F. De Angelis, C. Liberale, M.L. Coluccio, G. Cojoc, E. Di Fabrizio, Nanoscale 3 (2011) 2689–2696.
[23] F. De Angelis, G. Das, P. Candeloro, M. Patrini, M. Galli, A. Bek, M. Lazzarino, I. Maksymov, C. Liberale, L.C. Andreani, E. Di Fabrizio, Nature Nanotechnology 5 (2010) 67.
[24] P. Candeloro, L. Tirinato, N. Malara, A. Fregola, E. Casals, V. Puntes, G. Perozziello, F. Gentile, M.L. Coluccio, G. Das, C.Liberale, F. DeAngelis, E. Di Fabrizio, Analyst (in press), http://dx.doi.org/10.1039/c1an15313g.